

## Gyrobunching and wave–particle resonance in the lower hybrid drift instability

This content has been downloaded from IOPscience. Please scroll down to see the full text.

2011 Plasma Phys. Control. Fusion 53 074019

(<http://iopscience.iop.org/0741-3335/53/7/074019>)

View [the table of contents for this issue](#), or go to the [journal homepage](#) for more

Download details:

IP Address: 137.205.62.4

This content was downloaded on 22/01/2014 at 19:08

Please note that [terms and conditions apply](#).

# Gyrobunching and wave–particle resonance in the lower hybrid drift instability

J W S Cook<sup>1</sup>, R O Dendy<sup>1,2</sup> and S C Chapman<sup>1</sup>

<sup>1</sup> Centre for Fusion, Space and Astrophysics, Department of Physics, Warwick University, Coventry CV4 7AL, UK

<sup>2</sup> Euratom/CCFE Fusion Association, Culham Science Centre, Abingdon, Oxfordshire OX14 3DB, UK

E-mail: [j.w.s.cook@warwick.ac.uk](mailto:j.w.s.cook@warwick.ac.uk)

Received 15 December 2010, in final form 18 March 2011

Published 18 May 2011

Online at [stacks.iop.org/PPCF/53/074019](http://stacks.iop.org/PPCF/53/074019)

## Abstract

We report a first principles study of the coupled evolution of energetic ions, background majority ions, electrons and electromagnetic fields in magnetized plasma during the linear phase of the lower hybrid drift instability. A particle-in-cell code, with one spatial and three velocity space co-ordinates, is used to analyse the evolving distribution of a drifting ring-beam population of energetic protons in physical space and gyrophase angle. This analysis is carried out for bulk plasma parameters that approximate to core conditions in large tokamaks, with an energetic ion distribution that is motivated by observations of ion cyclotron emission and may be relevant to alpha channelling. Resonant energy transfer occurs at the two gyrophase angles at which the instantaneous speed of an energetic proton on its cyclotron orbit precisely matches the phase velocity of the lower hybrid wave along the simulation domain. Electron space-charge oscillations determine the wavelength of the propagating lower hybrid wave, and thereby govern the spatial distribution of gyrobunching of the energetic protons that drive the instability.

(Some figures in this article are in colour only in the electronic version)

## 1. Introduction

Understanding the nature of the wave–particle interaction that drives the lower hybrid drift instability (LHDI) [1–4] is of fundamental interest in plasma physics. The LHDI is potentially operative wherever drifting populations of ions (whether suprathermal minorities or arising from equilibrium gradients) occur in magnetized plasmas. There is an extensive literature documenting its many roles in both space [5–7] and, increasingly, laboratory [8, 9] plasma physics. Predominantly electrostatic waves, propagating quasi-perpendicular to the magnetic field, are preferentially excited by the LHDI. Their frequency is characterized by the lower hybrid frequency  $\omega_{\text{LH}} = (\Omega_{\text{ce}}\Omega_{\text{ci}}/(1 + \Omega_{\text{ce}}\Omega_{\text{ci}}/\omega_{\text{pi}}^2))^{1/2}$ , which exceeds the cyclotron

frequency of the ions and is below that of the electrons. It is clear from the foregoing that the LHDI possesses features that invite deeper investigation. The instability arises from the beam-like (i.e. directed in velocity space) character of the fast ion population that drives it, while the waves excited are conditioned by the cyclotronic (i.e. rotational in velocity space) natural frequency  $\Omega_{ci}$  of the background thermal ions. The waves excited are conditioned by the electron–ion mass ratio through  $\Omega_{ci}/\Omega_{ce}$ , implying that electron inertia plays a role. The waves excited are also conditioned by the density of charge carriers through the ion plasma frequency  $\omega_{pi}$ , implying that charge separation plays a central role.

In this paper we study the physics of the excitation mechanism of the LHDI, using a particle-in-cell (PIC) code [10–14] which provides a fully kinetic description of the interaction between minority ( $\sim 1\%$ ) energetic protons, background thermal deuterons, electrons, the self-consistent electromagnetic fields and the imposed background magnetic field. In particular, we focus on the dynamics of the ions as they drive the LHDI, which is found to exhibit coherent bunching that is highly structured in both velocity space and real space. To anticipate some key results, the kinetic treatment of both electrons and ions enables us to capture two essential features of the physics that are not addressed (because they are averaged over) in higher order reduced models. First, the code directly represents the excited waves as propagating electron charge density oscillations with well-defined frequency and wavelength. Second, the code directly represents ion motion and can therefore resolve the angular sector of an ion cyclotron orbit during which the ion is transiently in Doppler-shifted phase resonance with the wave that is being excited.

The scenario for the LHDI considered here is motivated by observations of radiative collective instability (ion cyclotron emission, ICE) of minority fusion-born and beam-injected energetic ions in the outer mid-plane edge plasma of the JET [15–17] and TFTR [18–20] tokamaks. Analysis of the spatial drift orbits of the ions responsible for exciting the fast Alfvén waves observed showed [15, 19] that their velocity space distribution can be approximated by the analytical model  $f(v_{\perp}, v_{\parallel}) = 1/(2\pi v_r)\delta(v_{\perp} - v_r)\delta(v_{\parallel} - u)$  where  $v_r$  and  $u$  correspond to a pitch angle just inside the trapped-passing boundary for an ion near its birth energy. In [21, 22] it was shown that these distributions can also be unstable against the LHDI. Furthermore, the lower hybrid waves excited were found to undergo Landau damping on resonant electrons asymmetrically with respect to the distribution of parallel velocities, resulting in the spontaneous creation of a current supported by suprathermal electrons [21, 22]. This is a key building block of alpha channelling [23, 24] scenarios for fusion plasmas. The principle of lower hybrid current drive by Landau damping of externally applied waves was identified by Fisch and colleagues [25, 26] for fusion plasmas, and an application to spacecraft and rocket-borne measurements of electron distributions in Earth’s auroral zone was noted in [27]. The JET and TFTR fusion plasma results motivate the present choice of plasma parameters, approximating a background plasma at a temperature similar to that found in the core of a large tokamak plasma; and energetic ion velocity distribution, relevant to ICE observations [15–20] and to recent simulations of LHDI alpha channelling [21, 22]. While these represent only one possible realization of an LHDI scenario, among many, we believe that the underlying physics of the phase resonant excitation described in this paper is generic to a significant extent.

## 2. Fundamentals of the simulation

Consider the unperturbed spatiotemporal orbit, during one cyclotron period, of a single energetic proton drawn from the energetic ion distribution  $f(v_{\perp}, v_{\parallel}) \sim \delta(v_{\perp} - v_r)\delta(v_{\parallel} - u)$ . Our simulation domain incorporates all three components of velocity  $v$ , but has only one spatial

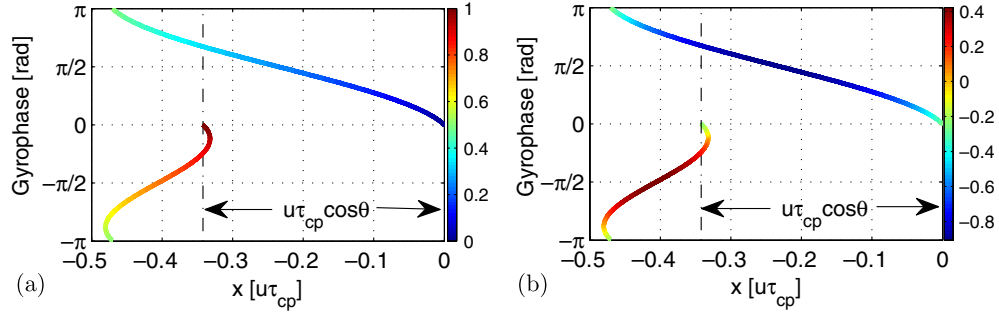


**Figure 1.** Projected motion of an energetic proton along the simulation domain direction  $x$  as a function of gyrophase  $\alpha$  during a single cyclotron orbit. In panel (a), shading (colour online) indicates time in units of proton gyroperiods; in panel (b), shading (colour online) indicates velocity in the  $x$  direction in units of initial proton speed. This motion is implicit in the definition of the unperturbed velocity distribution in terms of  $v_{\perp}$  and  $v_{\parallel}$ . The parallel velocity component present in this geometry causes a drift in  $x$  of  $u\tau_{cp}\cos\theta$  per gyro-orbit, where  $\tau_{cp} = 2\pi/\Omega_{cp}$  is the proton gyroperiod.

co-ordinate  $x$ , which is oriented at an arbitrary angle  $\theta$  with respect to the direction of the magnetic field  $B$ . We must determine the projection of the movement of each proton along the simulation domain  $x$ , with respect to gyrophase  $\alpha = \arctan(v_{\perp,1}/v_{\perp,2})$ , which takes the values  $\pm\pi/2$  when the proton passes through the plane defined by  $v_x$  and the component of  $v$  parallel to  $B$ . The  $x$ -projected motion of the proton is plotted as a function of gyrophase  $\alpha$  in figure 1, where its unperturbed instantaneous position is shown as a function of time, which is indicated by shading (colour online) in figure 1(a). Shading (colour online) in figure 1(b) indicates the corresponding instantaneous velocity along  $x$ . Together figures 1(a) and (b) provide the information necessary to show the relationship between position  $x$ , gyrophase  $\alpha$  and velocity  $v_x = dx/dt$  along the simulation domain of an unperturbed energetic proton. The combination of cyclotron motion and drift parallel to  $B$  results in the drift shown, which implies that the particle velocity  $v_x$  varies continuously. It follows that phase resonance between the particle  $v_x$  and any wave that can propagate with phase velocity  $\omega/k_x$  will only occur transiently, along a particular segment of the cyclotron orbit. It is in this segment that the perturbed ( $x, \alpha$ ) phase orbit of the ion resonantly exciting the wave will deviate most strongly from the unperturbed orbit of figure 1.

It is known from figures 3 and 4 of [21] that the dominant collectively excited modes propagate in the negative  $x$ -direction with  $\omega/k_x \sim 1.5 \times 10^{-7} \text{ m s}^{-1} \lesssim v_x = u \cos\theta - v_r \sin\theta$ . Modes with slightly lower amplitude are excited propagating in the opposite direction with similar phase speed. These phase velocities are located near the maxima of transient speeds, in either direction along the simulation domain, of the energetic ions that drive the instability. These maxima of transient speeds occur (see figure 1) at gyrophases  $\alpha = \pm\pi/2$ ; see also panel (a) of figure 2 of [22].

### 3. Simulation results

Let us first consider the physical character of the dominant wave that is excited in our simulations. Figure 2 plots the spatial distribution of the electrons at a snapshot in time towards the end of the linear phase of the instability. It confirms that the predominantly electrostatic wave is primarily a charge density oscillation supported by the electrons. The full

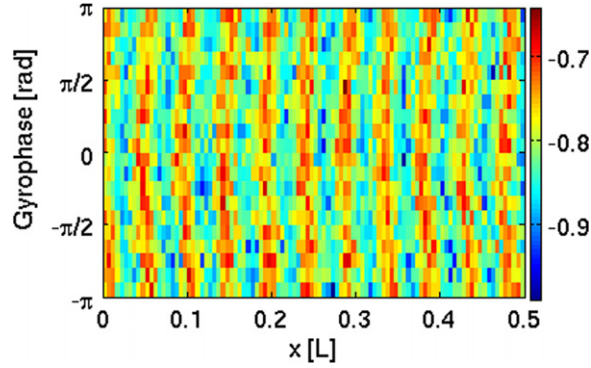


**Figure 2.** PIC code derived electron population data from a snapshot at  $t = 19.8\tau_{\text{LH}}$ , where  $\tau_{\text{LH}} = 2\pi/\omega_{\text{LH}}$ , towards the end of the linear stage of the instability. Electron probability density on a  $\log_{10}$  scale is indicated by shading (colour online) as a function of gyrophase (ordinate axis) and position (abscissa). Position axes are in units of box length  $L$  and gyrophase axes are in radians. The vertical stripes indicate that electron bunching occurs as a function of position and not gyrophase: electrons participate in wave action by charge density oscillation.

simulation domain accommodates 21 wavelengths of this lower hybrid wave, of which 10.5 are plotted in the half-box of figure 2 for reasons of pictorial resolution.

We now turn to the resonant interaction between the protons and the wave as manifested by the distribution of energetic protons along the physical co-ordinate  $x$  and with respect to gyrophase angle  $\alpha$ . Figure 3 plots (left) the whereabouts of protons in  $(x, \alpha)$  phase space at  $t = 19.8\tau_{\text{LH}}$ , towards the end of the linear phase of the LHDI in this scenario, and (right) the corresponding distribution of particle energies. Within the spatial limits of the simulation box, there are 21 gyrophase bunched structures which span the whole gyrophase range: 10.5 of these are visible in figure 3, because data from only half of the simulation domain are shown (figures 2–4 all show data from only half of the spatial domain). The simulation domain length  $L \simeq 6.3$  proton Larmor radii. This is sufficiently large that protons undergo  $\sim 7$  gyro-orbits per boundary crossing, which corresponds to approximately one boundary crossing per proton during the entire simulation. Figure 3 demonstrates that the rapidly varying behaviour of the distribution in the negative  $\alpha$  domain of phase space is a continuation of the slower variation in the positive domain. This new result is not apparent from previous analysis of the LHDI in this regime, for example figure 5 of [21] and figure 4 of [22].

Figure 3 (left) captures wave excitation by the energetic ions as it occurs. The asymmetry with respect to gyrophase arises from the differing strength of waves, self-consistently excited, with which an individual particle can resonate as it moves forwards and backwards in  $x$  with changing  $\alpha$ . The strong spatially dispersive distortion at  $\alpha = \pi/2$  corresponds (see figure 1) to the maximum negative particle velocity (see also figure 2(a) of [22]), which is located between the points in gyrophase where the resonant drive of the dominant backward-propagating waves takes place. The dominant wave packet (concentration of electromagnetic wave field in  $(\omega, k)$  space) arises self-consistently in the PIC simulation from collective motion of all the ions (energetic minority and thermal background) and the electrons, coupled to the electromagnetic field. The corresponding dominant wave's phase velocity need not exactly match the maximum instantaneous speed of any individual particle, and it is slightly smaller than the maximum speed of the protons. Consequently, there are two positions of resonance in gyrophase, either side of the maximum negative velocity. These resonant perturbations apparently condition the long-wavelength (in gyrophase  $\alpha$ ) structure across the positive- $\alpha$

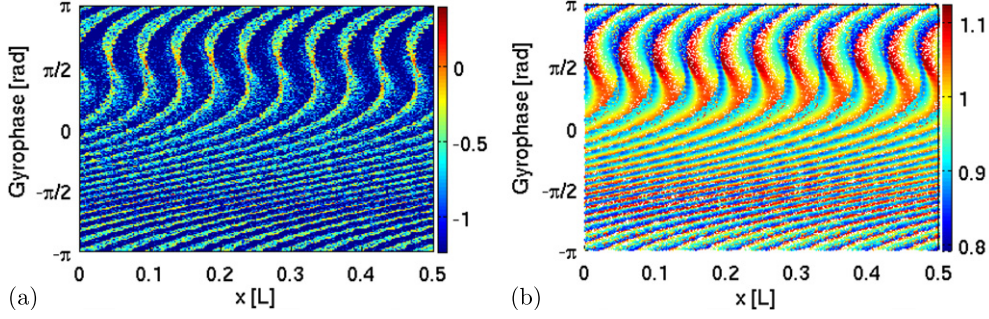


**Figure 3.** PIC code derived proton population data from a snapshot at  $t = 19.8\tau_{LH}$  towards the end of the linear stage of the instability, plotted as a function of gyrophase (ordinate axis) and position (abscissa). Position axes are in units of box length  $L$  and gyrophase axes are in radians. Panel (a): proton probability density on a  $\log_{10}$  scale indicated by shading (colour online). Panel (b): proton energy, in units of the initial proton energy, indicated by shading (colour online). Both panels show 10.5 nearly identical  $s$ -shaped features in the upper half plane at regular intervals in the spatial direction, as well as smaller scale repeating structures.

domain of phase space. At  $\alpha = -\pi/2$ , which corresponds to the maximum positive particle velocity, the consequences of resonance are apparent in the moiré pattern (which is more easily visible in figure 3 (right)). While both these velocity resonances give rise to significant (but differing by an order of magnitude) concentrations of electromagnetic field energy in  $(\omega, k)$ -space, as shown in figure 3 of [21], it follows from figure 3 that the phase space consequences are different in the two cases. The number of moiré  $s$ -shaped features in the lower half plane of figure 3 exceeds that in the upper half plane. This reflects the difference in  $k_x$  for the waves excited at the two resonances, see again figure 3 of [21].

Figure 3 (right) assists interpretation of the physics in terms of the simplified analytical model for the dynamics of the particle-wave interaction that was introduced in equations (12)–(16) of [22]. The essence of this model is that the impact of wave–particle interaction, for a proton with initial gyrophase  $\alpha_0$  at  $t = 0$  and at arbitrary  $(x, t)$ , scales with the magnitude of the electric field which that proton experienced when it was most closely in phase resonance with the wave. This resonance will have occurred at time  $t_R(\alpha_0)$  such that  $v_x(t_R) = \omega/k$ , where  $\omega \sim 6\omega_{LH}$  and  $k = -2\omega_{pe}/c$  are the angular frequency and wavenumber of the dominant excited mode in the simulation, obtained from the analysis of the Fourier transform of the electromagnetic field in figure 3 of [21]. Given an energetic proton moving on an unperturbed orbit drawn from the drifting beam distribution specified previously, expressions for  $t_R$  and position  $x_R(\alpha_0, x, t)$  follow from equations (14) and (15) of [22]. The key point is that the field amplitude,  $\mathcal{E}(\alpha_0, x, t)$  experienced at the point of resonance  $(x_R, t_R)$ , which is given by equation (16) of [22], is considered a property of the proton at all subsequent  $(x, t)$ . Figure 4 (left) plots  $\mathcal{E}(\alpha_0, x, t)$  for a population of energetic protons that is initially uniformly distributed in space  $x$  and gyrophase angle  $\alpha_0$  at an arbitrary time  $t = 2\pi/\Omega_{cp}$ . Figure 4 (right) is derived from the analytical model using the three waves identified from the Fourier transform of the excited electromagnetic field that is generated by the PIC simulation during its linear phase. To construct it we repeat the operation used for figure 4 (left) while adding: a second wave whose  $(\omega, k)$  are those identified as the harmonic of the dominant backward travelling wave in the Fourier transform ( $\omega_h = 12\omega_{LH}$ ,  $k_h = -4\omega_{pe}/c$ ), and whose amplitude is smaller by a factor ten; and a third wave whose  $(\omega, k)$  are those identified for the forward travelling excited wave in the Fourier transform ( $\omega_f = 6.6\omega_{LH}$ ,  $k_f = 1.3\omega_{pe}/c$ ), and whose amplitude is smaller by a factor four.

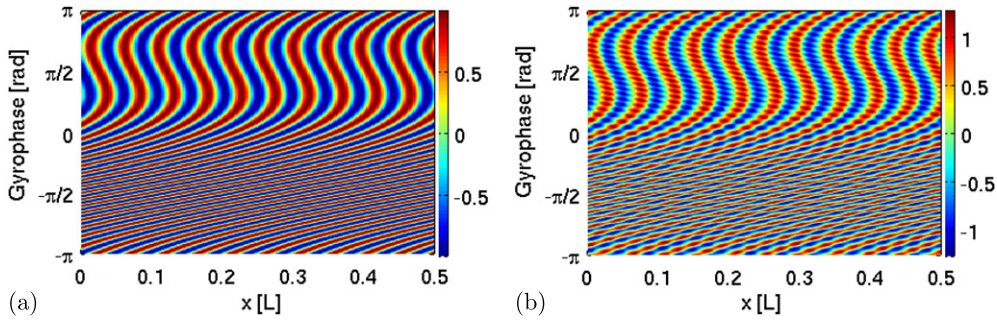


**Figure 4.** Normalized electric field amplitude  $\mathcal{E}$  indicated by shading (colour online) experienced by protons at their most recent point of resonance, as a function of proton gyrophase and position at a snapshot in time (see text). Panel (a): normalized wave amplitude seen by protons at resonance with the dominant wave. Panel (b): as panel (a) for the sum of dominant wave of unit amplitude, its second harmonic of one tenth amplitude, and a wave travelling in the opposite direction of one quarter amplitude. Data in panel (a) show the effect of resonance with the dominant excited wave as visible from the large scale structure in figures 3(a) and (b), while panel (b) shows finer scale structures, as in figure 3(b), highlighting the effects of resonances with less powerful excited waves.

Figure 4 (right) appears to capture the key features of figure 3 (right). This analytical model is based on unperturbed proton gyro-orbits, and figure 4 shows that these suffice to recreate gyro bunching effects seen in the PIC simulations. This is the case because perturbations are small in the sense that: the resonant gyrophase angles are sharply defined; and the spatial deviation (as distinct from gyrophase deviation) of the resonant particles from their unperturbed orbits is small compared with the wavelength of the excited waves.

#### 4. Conclusions

Analysis of the distribution in physical space and gyrophase angle of a drifting ring-beam population of energetic ions, as they drive the linear phase of the lower hybrid drift instability in a 1D3V PIC simulation, yields insights into the underlying plasma physics. The spatial coherence and spatial variation of the gyrophase bunched structures are shown to reflect a combination of cyclotron-type and beam-type dynamical and resonant effects, conditioned by the interplay of ion and electron dynamics. These new results shed fresh light on the hybrid character of the lower hybrid drift instability.

Resonant energy transfer occurs at the narrowly defined gyrophases at which the instantaneous speed of an energetic proton, from the drifting ring-beam population, on its cyclotron orbit precisely matches the phase velocity of the lower hybrid wave along the simulation domain. As in any resonant wave–particle instability, coupling to a wave that can propagate is necessary. In the present case, it is electron space-charge oscillation (figure 2) that determines the wavelength of the propagating lower hybrid wave, and thereby governs the spatial distribution of gyro bunching of the energetic protons (figures 3 and 4) that drive the instability. The gyrophase structure of phase space bunching at any given position is governed by the proton trajectories on their cyclotron orbits, which are oblique to the direction of propagation of waves along the simulation domain, in conjunction with restrictions on the spatial separation of gyro bunches due to collective electron oscillation.

Many of the key features of the wave–particle interaction that we observe in the simulations can be understood retrospectively in terms of a simplified analytical model. However the nature, value and number of parameters in this simplified model are wholly reliant on PIC

code outputs for their specification. It is the PIC code that yields the number of waves, their relative amplitudes, and their frequencies and wavenumbers.

Our results rest on a hybrid resonance: a beam-type resonance that is localized to a short angular segment of the gyro-orbit. Our results thereby capture the key physics of the lower hybrid drift instability. The specifics of this interaction, including the duration of particle transit through the segment of its gyro-orbit where the interaction takes place, will depend on plasma parameters. We note that the instantaneous approximation for the resonant interaction (figure 4) works well, suggesting that dependence on the duration of the resonant interaction—already captured by the PIC code—is weak.

Our choice of plasma parameters reflects a hypothetical alpha channelling [21, 22] scenario where drifting ring-beam energetic ions exist in a background plasma at a temperature similar to that found in the core of a large tokamak plasma. While the physics is generic, we note that this scenario is motivated by observations of ion cyclotron emission from JET [15] and TFTR [19].

### Acknowledgments

This work, part-funded by the European Communities under the contract of Association between EURATOM and CCFE, was partly carried out within the framework of the European Fusion Development Agreement. The views and opinions expressed herein do not necessarily reflect those of the European Commission. This work was also part-funded by the RCUK Energy Programme under grant EP/I501045. This project used the EPOCH code developed under EPSRC grant EP/G054950/1 and the authors thank Christopher Brady and the EPOCH development team. The authors also thank Nathaniel Fisch for helpful conversations.

Euratom © 2011.

### References

- [1] Davidson R C, Gladd N T, Wu C S and Huba J D 1977 Effects of finite plasma beta on the lower-hybrid-drift instability *Phys. Fluids* **20** 301–10
- [2] Hsia J B, Chiu S M, Hsia M F, Chou R L and Wu C S 1979 Generalized lower-hybrid-drift instability *Phys. Fluids* **22** 1737–46
- [3] Silveira O J G, Ziebell L F, Gaelzer R and Yoon P H 2002 Unified formulation for inhomogeneity-driven instabilities in the lower-hybrid range *Phys. Rev. E* **65** 036407
- [4] Daughton W, Lapenta G and Ricci P 2004 Nonlinear evolution of the lower-hybrid drift instability in a current sheet *Phys. Rev. Lett.* **93** 105004
- [5] Dobe Z, Quest K B, Shapiro V D, Szego K and Huba J D 1999 Interaction of the solar wind with unmagnetized planets *Phys. Rev. Lett.* **83** 260–3
- [6] Yoon P H, Lui A T Y and Chang C-L 1994 Lower-hybrid-drift instability operative in the geomagnetic tail *Phys. Plasmas* **1** 3033–43
- [7] Drake J F, Guzdar P N, Hassam A B and Huba J D 1984 Nonlinear mode coupling theory of the lower-hybrid-drift instability *Phys. Fluids* **27** 1148–59
- [8] Gladd N T 1976 The lower hybrid drift instability and the modified two stream instability in high density theta pinch environments *Plasma Phys.* **18** 27–40
- [9] Carter T A, Ji H, Trintchouk F, Yamada M and Kulsrud R M 2001 Measurement of lower-hybrid drift turbulence in a reconnecting current sheet *Phys. Rev. Lett.* **88** 015001
- [10] Devine P E, Chapman S C and Eastwood J W 1995 One- and two-dimensional simulations of whistler mode waves in an anisotropic plasma *J. Geophys. Res.—Space Phys.* **100** 17189–204
- [11] Oppenheim M, Newman D L and Goldman M V 1999 Evolution of electron phase-space holes in a 2D magnetized plasma *Phys. Rev. Lett.* **83** 2344–7
- [12] Dieckmann M E, Chapman S C, Ynnerman A and Rowlands G 1999 The energy injection into waves with a zero group velocity *Phys. Plasmas* **6** 2681–92

- [13] Birch P C and Chapman S C 2001 Detailed structure and dynamics in particle-in-cell simulations of the lunar wake *Phys. Plasmas* **8** 4551–9
- [14] Birch P C and Chapman S C 2001 Particle-in-cell simulations of the lunar wake with high phase space resolution *Geophys. Res. Lett.* **28** 219
- [15] Cottrell G A and Dendy R O 1988 Superthermal radiation from fusion products in JET *Phys. Rev. Lett.* **60** 33–36
- [16] Cottrell G A, Bhatnagar V P, Da Costa O, Dendy R O, Jacquinot J, McClements K G, McCune D C, Nave M F F, Smeulders P and Start D F H 1993 Ion cyclotron emission measurements during JET deuterium-tritium experiments *Nucl. Fusion* **33** 1365–87
- [17] McClements K G, Hunt C, Dendy R O and Cottrell G A 1999 Ion cyclotron emission from JET D-T plasmas *Phys. Rev. Lett.* **82** 2099–102
- [18] Dendy R O, McClements K G, Lashmore-Davies C N, Cottrell G A, Majeski R and Cauffman S 1995 Ion cyclotron emission due to collective instability of fusion products and beam ions in TFTR and JET *Nucl. Fusion* **35** 1733–42
- [19] Cauffman S, Majeski R, McClements K G and Dendy R O 1995 Alfvénic behaviour of alpha particle driven ion cyclotron emission in TFTR *Nucl. Fusion* **35** 1597–602
- [20] McClements K G, Dendy R O, Lashmore-Davies C N, Cottrell G A, Cauffman S and Majeski R 1996 Interpretation of ion cyclotron emission from sub-Alfvénic fusion products in the Tokamak Fusion Test Reactor *Phys. Plasmas* **3** 543–53
- [21] Cook J W S, Chapman S C and Dendy R O 2010 Electron current drive by fusion-product-excited lower hybrid drift instability *Phys. Rev. Lett.* **105** 255003
- [22] Cook J W S, Chapman S C, Dendy R O and Brady C S 2011 *Plasma Phys. Control. Fusion* submitted (arXiv:1010.2099v1 [physics.plasm-ph])
- [23] Fisch N J and Rax J-M 1992 Interaction of energetic alpha particles with intense lower hybrid waves *Phys. Rev. Lett.* **69** 612–5
- [24] Fisch N J 2010 Transformer recharging with alpha channeling in tokamaks *J. Plasma Phys.* **76** 627–34
- [25] Fisch N J 1978 Confining a tokamak plasma with rf-driven currents *Phys. Rev. Lett.* **41** 873–6
- [26] Karney C F F, Fisch N J and Jobs F C 1985 Comparison of the theory and the practice of lower-hybrid current drive *Phys. Rev. A* **32** 2554–6
- [27] Dendy R O, Harvey B M, O’Brien M and Bingham R 1995 Fokker-Planck modeling of auroral wave-particle interactions *J. Geophys. Res.* **100** 21973–8